# Multidimensional Potential Surfaces from the Direct Inversion of Probability Density and Energy Spectral Data[†]

**Wusheng Zhu and Herschel Rabitz\***

*Department of Chemistry, Princeton University, Princeton, New Jersey 08544-1009*

*Received: January 26, 2000; In Final Form: May 18, 2000*

This paper presents a direct potential surface inversion algorithm for multidimensional quantum systems based on combining probability density and energy spectral data. The algorithm expresses the potential explicitly in terms of the eigenstate probability density and the associated eigenenergies. Simulations show that the inversion can produce excellent results in the regular domain away from the asymptotic unidentifiable regions. The regular invertible domain of the potential can be adjusted by utilizing suitable spectral data. The inversion algorithm is successfully simulated to extract the potential surfaces of several one- and two-dimensional model systems.

## 1. Introduction

Potential energy surfaces (PES) are valuable for understanding intra- and intermolecular dynamics. Ab initio quantum chemistry calculations[1,2] can generate a PES, however, extensive computational effort is required to attain high accuracy results. The traditional inversion of time independent data (e.g., cross sections, energy spectra)[3−8] requires the iterative solution of complex equations, which is especially difficult for multidimensional systems.

Recent progress in ultrafast laser technology[9] is beginning to make it possible to measure the probability density data of either a time dependent wave packet (temporal and spatial resolution)[10] or a stationary eigenstate (spatial resolution).[11] There are a number of emerging measurement methods for obtaining the probability density data, including laser pump-dump electron diffraction,[12] ultrafast X-ray diffraction,[13] photoexcitation followed by autoionization of a core state,[14] ultrafast photoelectron spectra,[15] and Coulomb explosion imaging.[16,17] Although data of the quality needed for inversion are not yet in hand, the fervent laboratory activity warrants the development of suitable algorithms to extract the full physical information content in anticipation of its forthcoming availability. In this spirit, the present paper explores the feasibility of achieving high quality inversion from time independent probability density data combined with associated spectral absorptions.

In this paper, a new time independent inversion algorithm will be explored, which is particularly designed to treat emerging high spatial resolution probability density imaging data.[11] As a background initial step, section 2 develops a uniform time dependent inversion algorithm, whose one-dimensional case was introduced elsewhere.[18] Section 3 will investigate some possible time independent algorithms, and particularly emphasize an inversion algorithm which is very fast and stable. Finally, in section 4, several one- and two-dimensional model systems will be tested in inversion simulations applying the time independent algorithm to extract the underlying potential surfaces.

## 2. Time Dependent Inversion Algorithm

Several time dependent inverse algorithms have been introduced for treating different types of time dependent data, such

---

as ultrafast pump−probe spectroscopic data,[19] the time dependent expectation value (i.e., trajectory data) of a certain operator,[20] and time dependent wave packet imaging data.[21] Each of these approaches has its own strengths and limitations. Here we will show that it is feasible to develop an inversion algorithm for a system with a multidimensional potential based on time dependent probability density data. This kind of data is less demanding to obtain than wave packet imaging data, and it is easier to use for extracting the potential than the effort involved with spectroscopic data. The following time dependent inversion algorithm also will lay the foundation of its counterpart time independent inversion algorithm in section 3.

For an *N*-dimensional quantum system, the time dependent Schrödinger equation is

$$\left[-\frac{1}{2}\nabla^2 + V(\mathbf{x})\right]\psi(\mathbf{x}, t) = i\frac{\partial}{\partial t}\psi(\mathbf{x}, t) \tag{1}$$

where $\mathbf{x} \equiv \{x_1, x_2, ..., x_N\}$. The Laplacian is defined as $\nabla^2 \equiv \sum_{i=1}^{N} \partial^2/\partial\hat{x}_i^2$ in terms of a set of mass-weighted coordinates $\hat{x}_i = \sqrt{\mu_i}\, x_i$, $i = 1, 2, ..., N$. $V(\mathbf{x})$ is the multidimensional potential, and $\psi(\mathbf{x}, t)$ is the time dependent wave function. The wave function is expressed as $\psi(\mathbf{x}, t) = \sqrt{\rho(\mathbf{x},t)} \exp[iS(\mathbf{x}, t)]$, where the real function $\rho(\mathbf{x}, t)$ is the probability density and the real function $S(\mathbf{x}, t)$ is the phase. Equation 1 is equivalent to hydrodynamic coupled equations[22] except possibly at nodal points [where $\rho(\mathbf{x}, t) = 0$, this leaves $S(\mathbf{x}, t)$ indeterminate]:

$$\nabla\cdot[\rho(\mathbf{x}, t)\nabla S(\mathbf{x}, t)] = -\frac{\partial\rho(\mathbf{x}, t)}{\partial t} \tag{2}$$

$$\frac{1}{2}[\nabla S(\mathbf{x}, t)]^2 + V(\mathbf{x}) - \frac{1}{2}\frac{\nabla^2\sqrt{\rho(\mathbf{x}, t)}}{\sqrt{\rho(\mathbf{x}, t)}} = -\frac{\partial S(\mathbf{x}, t)}{\partial t} \tag{3}$$

Since only the probability density $\rho(\mathbf{x}, t)$ is assumed to be available data, while the phase $S(\mathbf{x}, t)$ is unknown, then the inversion for potential from eqs 2 and 3 has to map out the relationship between the potential and the probability density. Taking the gradient of both sides of eq 3 and utilizing eq 2 will lead to the following equation:

---

[†] Part of the special issue "Thomas Spiro Festschrift".

$$\rho(\mathbf{x}, t)\nabla V(\mathbf{x}) = \frac{1}{4}\nabla[\nabla^2\rho(\mathbf{x}, t)] -$$
$$\frac{1}{4}[\nabla\rho(\mathbf{x}, t)\cdot\nabla + \nabla\cdot\nabla\rho(\mathbf{x}, t)]\nabla\ln\rho(\mathbf{x}, t) -$$
$$([\rho(\mathbf{x}, t)\nabla S(\mathbf{x}, t)]\cdot\nabla + \nabla\cdot[\rho(\mathbf{x}, t)\nabla S(\mathbf{x}, t)])\nabla S(\mathbf{x}, t) -$$
$$\frac{\partial[\rho(\mathbf{x}, t)\nabla S(\mathbf{x}, t)]}{\partial t} \quad (4)$$

Considering the asymptotic zero boundary condition of the probability density, the spatial integration of eq 4 yields

$$\int_{R^N} \rho(\mathbf{x}, t)\nabla V(\mathbf{x})\, d\mathbf{x} = -\frac{\partial}{\partial t}\int_{R^N} \rho(\mathbf{x}, t)\nabla S(\mathbf{x}, t)\, d\mathbf{x} \quad (5)$$

where the integral identity

$$\int_{R^N} (\nabla\cdot\vec{B} + \vec{B}\cdot\nabla)\vec{A}\, d\mathbf{x} = \oint_S \vec{A}(\vec{B}\cdot d\vec{S}) \quad (6)$$

has been utilized. Denoting the spatial vector as $\vec{x} \equiv x_1\vec{e}_1 + x_2\vec{e}_2 + ... + x_N\vec{e}_N$, we have

$$-\frac{\partial^2}{\partial t^2}\int_{R^N} \vec{x}\rho(\mathbf{x}, t)\, d\mathbf{x} = \frac{\partial}{\partial t}\int_{R^N} \vec{x}\nabla\cdot[\rho(\mathbf{x}, t)\nabla S(\mathbf{x}, t)]\, d\mathbf{x}$$
$$= -\frac{\partial}{\partial t}\int_{R^N} [\rho(\mathbf{x}, t)\nabla S(\mathbf{x}, t)\cdot\nabla]\vec{x}\, d\mathbf{x}$$
$$= -\frac{\partial}{\partial t}\int_{R^N} \rho(\mathbf{x}, t)\nabla S(\mathbf{x}, t)\, dx \quad (7)$$

where eqs 2 and 6 have been utilized. From eq 7, we see that eq 5 is equivalent to

$$\int_{R^N} \rho(\mathbf{x}, t)\nabla V(\mathbf{x})\, d\mathbf{x} = -\frac{\partial^2}{\partial t^2}\int_{R^N} \vec{x}\rho(\mathbf{x}, t)\, d\mathbf{x} \quad (8)$$

Equation 8 is a multidimensional version of Ehrenfest's relation, which produces a time dependent inversion algorithm of the multidimensional potential using only time dependent probability density data. Its one-dimensional version has been successfully applied in simulations.[18] For multidimensional cases, in principle the inversion algorithm is feasible as well. However, inversion of the kernel in a multidimensional integral would require much more computational effort, and the ill-posedness of the problem may call for additional care to treat. This paper aims to develop a more rapid and less singular inversion algorithm. The following treatment investigates various alternative time independent inversion algorithms. In this regard, the result in eq 8 may be derived by other means, but the route taken here is useful as it lays the foundation for comparison with the approach in section 3 below.

## 3. Time Independent Inversion Algorithm

Following the same spirit in deriving the above time dependent algorithm, we also establish an alternative time independent inversion algorithm. For an *N*-dimensional quantum system, the time independent Schrödinger equation is

$$\left[-\frac{1}{2}\nabla^2 + V(\mathbf{x})\right]\psi(\mathbf{x}) = E\psi(\mathbf{x}) \quad (9)$$

where $\psi(\mathbf{x})$ is an eigenstate with energy $E$. The general solution of eq 9 can be written as $\psi(\mathbf{x}) = \sqrt{\rho(\mathbf{x})}\exp[iS(\mathbf{x})]$ where the real function $\rho(\mathbf{x})$ is the probability density and the real function

$S(\mathbf{x})$ is the phase. Equation 9 is equivalent to the coupled equation of the real and imaginary parts, leaving the nodal points undetermined:

$$\nabla\cdot[\rho(\mathbf{x})\nabla S(\mathbf{x})] = 0 \quad (10)$$

$$\frac{1}{2}[\nabla S(\mathbf{x})]^2 + V(\mathbf{x}) - \frac{1}{2}\frac{\nabla^2\sqrt{\rho(\mathbf{x})}}{\sqrt{\rho(\mathbf{x})}} = E \quad (11)$$

By following logic similar to the time dependent formulation in eq 8, a time independent inversion algorithm can be constructed. Combining eqs 10 and 11 produces

$$\frac{1}{4}\nabla\cdot(\rho(\mathbf{x})\nabla[S(\mathbf{x})]^2) + \rho(\mathbf{x})\, V(\mathbf{x}) -$$
$$\frac{1}{4}\nabla^2\rho(\mathbf{x}) + \frac{1}{8}\frac{[\nabla\rho(\mathbf{x})]^2}{\rho(\mathbf{x})} = \rho(\mathbf{x})E \quad (12)$$

For bound states, integrating eq 12 over all space and utilizing Green's theorem along with the boundary conditions will produce

$$\int_{R^N} \rho(\mathbf{x})V(\mathbf{x})\, d\mathbf{x} = E - \frac{1}{8}\int_{R^N} \frac{[\nabla\rho(\mathbf{x})]^2}{\rho(\mathbf{x})}\, d\mathbf{x} \quad (13)$$

Equation 13 provides a relationship between the potential, bound state probability density and the associated energy. From another point of view, eq 13 shows that the energy only depends on the probability density, rather than the wave function itself, which is the basis of density functional theory.

Unlike the time dependent algorithm based on eq 8, eq 13 is not directly suitable for potential inversion, which may be shown as follows. From eqs 10 and 11, we also have

$$\rho(\mathbf{x})\nabla V(\mathbf{x}) = \frac{1}{4}\nabla[\nabla^2\rho(\mathbf{x})] -$$
$$\frac{1}{4}[\nabla\rho(\mathbf{x})\cdot\nabla + \nabla\cdot\nabla\rho(\mathbf{x})]\nabla\ln\rho(\mathbf{x}) -$$
$$([\rho(\mathbf{x})\nabla S(\mathbf{x})]\cdot\nabla + \nabla\cdot[\rho(\mathbf{x})\nabla S(\mathbf{x})])\nabla S(\mathbf{x}) \quad (14)$$

which is just the time independent analogue of eq 4. Full space integration of eq 14 yields

$$\int_{R^N} \rho(\mathbf{x})\nabla V(\mathbf{x})\, d\mathbf{x} = 0 \quad (15)$$

which also can be deduced from eq 8 when $\rho$ is not time dependent. Therefore, combining eqs 15 and 13 gives

$$\int_{R^N} \rho(\mathbf{x})[V(\mathbf{x}) + \vec{c}\cdot\nabla V(\mathbf{x})]\, d\mathbf{x} = E - \frac{1}{8}\int_{R^N} \frac{[\nabla\rho(\mathbf{x})]^2}{\rho(\mathbf{x})}\, d\mathbf{x} \quad (16)$$

where $\vec{c}$ is an arbitrary constant vector. It can be seen from eq 16 that the potential inversion based on eq 13 using bound state probability density and energy data is not well posed. From the same probability density and energy data, the inverted potential would likely be contaminated with its gradient. To relieve this situation, more independent integral relationships between the potential and the bound state probability density and energy data need to be introduced. For example, an additional independent integral relationship from the virial theorem is

$$\int_{R^N} \rho(\mathbf{x})\, \vec{x}\cdot\nabla V(\mathbf{x})\, d\mathbf{x} = \frac{1}{4}\int_{R^N} \frac{[\nabla\rho(\mathbf{x})]^2}{\rho(\mathbf{x})}\, d\mathbf{x} \quad (17)$$

Inversion Algorithm for Quantum Systems

*J. Phys. Chem. B, Vol. 104, No. 46, 2000* **10865**

However, by following this route, the time independent multidimensional potential inversion algorithm is more complex, and the degree of relief of the global indetermination of the potential is not clear. It is important to appreciate that the global uncertainty in $V(\mathbf{x})$ by inversion of eq 13 is not intrinsic, as demonstrated later.

The reason that the apparently similar time dependent algorithm based on eq 8 is free of such global uncertainty lies in the fact that the time dependent probability density additionally preserves some relative phase information between the stationary states. For example, if a time dependent wave packet is a superposition of a number of bound states,

$$\psi(\mathbf{x}, t) = \sum_{\{\mathbf{j}\}} a_{\{\mathbf{j}\}}(t)\, \psi_{\{\mathbf{j}\}}(\mathbf{x}) \tag{18}$$

where $\{\mathbf{j}\}$ is the set of quantum numbers describing the multidimensional quantum states, then the time dependent probability density becomes

$$\rho(\mathbf{x}, t) = \sum_{\{\mathbf{j}\}\neq\{\mathbf{j}'\}}\sum_{\{\mathbf{j}'\}} a^*_{\{\mathbf{j}\}}(t)\, a_{\{\mathbf{j}'\}}(t)\sqrt{\rho_{\{\mathbf{j}\}}(\mathbf{x})\,\rho_{\{\mathbf{j}'\}}(\mathbf{x})} \times$$
$$\exp(i[S_{\{\mathbf{j}'\}}(\mathbf{x}) - S_{\{\mathbf{j}\}}(\mathbf{x})]) + \sum_{\{\mathbf{j}\}}|a_{\{\mathbf{j}\}}(t)|^2\, \rho_{\{\mathbf{j}\}}(\mathbf{x}) \tag{19}$$

where the relative phases between the bound states do not vanish. In the time independent algorithm, the bound state phase is completely lost. In the following treatment, we will explore a new time independent inversion algorithm utilizing the same probability density and energy data but without this global uncertainty.

Since the Hamiltonian is Hermitian, and the eigenvalues $E$ are real, then the eigenfunctions $\psi(\mathbf{x})$ in eq 9 can be always chosen to be real (there are special circumstances with unusual or incomplete boundary conditions leading to exceptions which will not be considered further here). From the definition, $\psi(\mathbf{x}) = \sqrt{\rho(\mathbf{x})}\,\exp[iS(\mathbf{x})]$, the real nature of the wave function requires

$$\sqrt{\rho(\mathbf{x})}\,\sin[S(\mathbf{x})] = 0 \tag{20}$$

Equation 20 implies that (i) if $\rho(\mathbf{x}) \neq 0$, then $S(\mathbf{x}) = n(\mathbf{x})\pi$, where the value of $n(\mathbf{x})$ may jump from one integer to another upon passing a nodal point, and (ii) if $\rho(\mathbf{x}) = 0$, then $S(\mathbf{x})$ is indeterminate.

From the definition, $\psi(\mathbf{x}) = \sqrt{\rho(\mathbf{x})}\,\exp[iS(\mathbf{x})]$, the following relationship holds generally even at nodal points, when the physical requirements on the continuity of the wave function and its gradient are considered:

$$\psi^*(\mathbf{x})\nabla\psi(\mathbf{x}) = \frac{1}{2}\nabla\rho(\mathbf{x}) + i\rho(\mathbf{x})\nabla S(\mathbf{x}) \tag{21}$$

When the wave function is real, eq 21 indicates that

$$\rho(\mathbf{x})\nabla S(\mathbf{x}) = 0 \tag{22}$$

Therefore, multiplying $[\rho(\mathbf{x})]^2$ on both sides of eq 11, and considering eq 22, we can formulate the inversion algorithm for multidimensional systems as

$$V(\mathbf{x}) = \frac{\frac{1}{4}\rho(\mathbf{x})\nabla^2\rho(\mathbf{x}) - \frac{1}{8}[\nabla\rho(\mathbf{x})]^2 + [\rho(\mathbf{x})]^2 E}{[\rho(\mathbf{x})]^2} \tag{23}$$

Alternatively, eq 23 may be derived directly from the Schrödinger equation (9) taking the wave function as real.

An additional issue is that multidimensional systems often exhibit degeneracies. For example, in a two-dimensional uncoupled isotropic harmonic oscillator, the two eigenstates, $\phi_1\phi_1$ and $\phi_0\phi_2$, have the same energy, where the subscripts indicate the quantum numbers associated with each degree of freedom. For this simple case, the degenerate eigenstates could be distinguished by separate excitation with two $\omega_{01}$ photons or by one $\omega_{02}$ photon. However, for more complicated situations, a superposition of the degenerate eigenstates will be accessed. The superposition state still has the same energy, but the probability density is very different from each pure degenerate eigenstate. The question is whether the superposition probability density can be used to invert the true potential; an analysis is presented below. We define an arbitrary superposition of a set of real degenerate eigenstates with the same energy as

$$\bar{\psi}(\mathbf{x}) = \sum_{\{\nu\}} b_{\{\nu\}}\, \psi_{\{\nu\}}(\mathbf{x}) \tag{24}$$

where $\{\nu\}$ are quantum numbers prescribing one of the degenerate eigenstates, and the real constants $b_{\{\nu\}}$ are subject to a normalization condition. Since each pure eigenfunction satisfies the Schrödinger equation (eq 9), it is obvious that the linear superposition state in eq 24 also satisfies the same equation:

$$\left[-\frac{1}{2}\nabla^2 + V(\mathbf{x})\right]\bar{\psi}(\mathbf{x}) = E\bar{\psi}(\mathbf{x}) \tag{25}$$

Denoting the superposition state by a new probability density and phase as $\bar{\psi}(\mathbf{x}) = \sqrt{\bar{\rho}(\mathbf{x})}\,\exp[i\,\bar{S}(\mathbf{x})]$, we will similarly obtain that the potential can be inverted in the same manner of eq 23 by the superposition probability density:

$$V(\mathbf{x}) = \frac{\frac{1}{4}\bar{\rho}(\mathbf{x})\nabla^2\,\bar{\rho}(\mathbf{x}) - \frac{1}{8}[\nabla\bar{\rho}(\mathbf{x})]^2 + [\bar{\rho}(\mathbf{x})]^2\, E}{[\bar{\rho}(\mathbf{x})]^2} \tag{26}$$

Another issue to consider is the nodal surfaces where $\rho(\mathbf{x}) = 0$ in eq 23. One way to remove the singular problem along the nodal surfaces is by combining a few observed eigenstate probability densities. In most cases, the combined result will be free of nodal surfaces, since the nodal surfaces will likely scatter in different ways for different eigenstates. The inversion algorithm can be implemented by

$$V(\mathbf{x}) =$$
$$\frac{\displaystyle\sum_{\{\lambda\}=\{\lambda_1\}}^{\{\lambda_2\}} c_{\{\lambda\}}\left[\frac{1}{4}\rho_{\{\lambda\}}(\mathbf{x})\nabla^2\rho_{\{\lambda\}}(\mathbf{x}) - \frac{1}{8}[\nabla\rho_{\{\lambda\}}(\mathbf{x})]^2 + [\rho_{\{\lambda\}}(\mathbf{x})]^2 E_{\{\lambda\}}\right]}{\displaystyle\sum_{\{\lambda\}=\{\lambda_1\}}^{\{\lambda_2\}} c_{\{\lambda\}}[\rho_{\{\lambda\}}(\mathbf{x})]^2}$$
$$\tag{27}$$

where $c_{\{\lambda\}}$ is a set of arbitrarily chosen positive weight coefficients. In some cases, the eigenstates may share one or more nodal isolated points or lines. If the discretized probability density is sampled very close to such nodal isolated points or lines, the inverted potential surface may exhibit unusual features which would be readily recognized. We can plot the probability density and single out those shared nodal points or lines, then sample the probability density again on a different grid to avoid

those shared nodal points or lines, which will get rid of such singularities.

The inversion algorithm in eq 27 is stable with respect to perturbative noisy experimental data. The norm analysis below will show the disturbance of the inverted potential, $\delta V(\mathbf{x})$, in response to a perturbation of the probability density and eigenenergy data, $\delta\rho_{\{\lambda\}}(\mathbf{x})$ and $\delta E_{\{\lambda\}}$. From eq 27, we have

$$
\frac{\|\delta V(\mathbf{x})\|}{\|V(\mathbf{x})\|} = \frac{\left\|\sum_{\{\lambda\}=\{\lambda_1\}}^{\{\lambda_2\}}\left(\frac{\delta V(\mathbf{x})}{\delta\pi_{\{\lambda\}}(\mathbf{x})}\delta\rho_{\{\lambda\}}(\mathbf{x}) + \frac{\delta V(\mathbf{x})}{\delta E_{\{\lambda\}}}\delta E_{\{\lambda\}}\right)\right\|}{\|V(\mathbf{x})\|} \leq
$$
$$
\frac{\sum_{\{\lambda\}=\{\lambda_1\}}^{\{\lambda_2\}}\left(\left\|\frac{\delta V(\mathbf{x})}{\delta\rho_{\{\lambda\}}(\mathbf{x})}\right\|\|\delta\rho_{\{\lambda\}}(\mathbf{x})\| + \left\|\frac{\delta V(\mathbf{x})}{\delta E_{\{\lambda\}}}\right\|\|\delta E_{\{\lambda\}}\|\right)}{\|V(\mathbf{x})\|} \tag{28}
$$

where

$$
\frac{\delta V(\mathbf{x})}{\delta E_{\{\lambda\}}} = \frac{c_{\{\lambda\}}[\rho_{\{\lambda\}}(\mathbf{x})]^2}{\sum_{\{\lambda\}=\{\lambda_1\}}^{\{\lambda_2\}} c_{\{\lambda\}}[\rho_{\{\lambda\}}(\mathbf{x})]^2} \tag{29}
$$

and

$$
\frac{\delta V(\mathbf{x})}{\delta\rho_{\{\lambda\}}(\mathbf{x})} =
$$
$$
\frac{\frac{1}{4}c_{\{\lambda\}}\left[\nabla^2\rho_{\{\lambda\}}(\mathbf{x}) + \rho_{\{\lambda\}}(\mathbf{x})\frac{\nabla^2\delta\rho_{\{\lambda\}}(\mathbf{x})}{\delta\rho_{\{\lambda\}}(\mathbf{x})} - \nabla\rho_{\{\lambda\}}(\mathbf{x})\frac{\nabla\delta\rho_{\{\lambda\}}(\mathbf{x})}{\delta\rho_{\{\lambda\}}(\mathbf{x})} + 8\rho_{\{\lambda\}}(\mathbf{x})E_{\{\lambda\}}\right]}{\sum_{\{\lambda\}=\{\lambda_1\}}^{\{\lambda_2\}} c_{\{\lambda\}}[\rho_{\{\lambda\}}(\mathbf{x})]^2} -
$$
$$
\frac{2c_{\{\lambda\}}{}^2\rho_{\{\lambda\}}(\mathbf{x})\left[\frac{1}{4}\rho_{\{\lambda\}}(\mathbf{x})\nabla^2\rho_{\{\lambda\}}(\mathbf{x}) - \frac{1}{8}[\nabla\rho_{\{\lambda\}}(\mathbf{x})]^2 + [\rho_{\{\lambda\}}(\mathbf{x})]^2 E_{\{\lambda\}}\right]}{\left(\sum_{\{\lambda\}=\{\lambda_1\}}^{\{\lambda_2\}} c_{\{\lambda\}}[\rho_{\{\lambda\}}(\mathbf{x})]^2\right)^2} \tag{30}
$$

The first- and second-order derivatives of the noisy probability density on the RHS of eq 30 will increase the norm of $\delta V(\mathbf{x})/\delta\rho_{\{\lambda\}}(\mathbf{x})$ to some degree. The first- and second-order derivatives of the noisy data may be evaluated by three-point finite differences with optimal intervals.[18] Thus, it can be relatively stable to obtain the low order derivatives of the noisy data. Therefore, $\delta V(\mathbf{x})/\delta\rho_{\{\lambda\}}(\mathbf{x})$ will be finite and only subject to modest disturbance, and then eq 28 shows that small perturbations in the probability density and eigenenergy data will result in small perturbations in the inverted potential in those regions where the combined denominator in eq 27 has significant magnitude.

Finally, it is evident that the invertible region depends on the combination of specific eigenstates. The combination of a number of eigenstates serves two purposes. One is to remove nodal surfaces. The other is to enlarge the invertible region. The actual number of combined eigenstates is not very important, and simply adding in more eigenstates may not significantly enlarge the invertible region. Furthermore, in a combination of a large number eigenstates, a portion of them
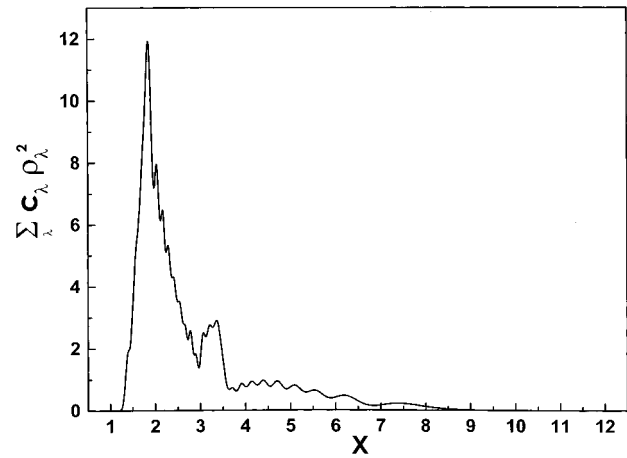


**Figure 1.** Spatial distribution of the denominator in the inversion formula for the first simulation example with perfect data. The significantly nonzero region defines the invertible domain, whose range is adjustable by using different eigenstates.

may be of little value. Dropping off this part may not affect the status of the nodal surfaces, as well as the invertible region. Usually, lower eigenstates have a narrow invertible region but less nodal surfaces, while higher eigenstates are of opposite character. A combination of a few low and high eigenstates should be very efficient, while the inclusion of intermediate eigenstates may have little contribution to either removing nodal surfaces or enlarging the invertible region. In practice, each case will have its own special characteristics.

## 4. Simulated Inversion

The purpose of the simulations is to test the behavior of the algorithm developed in section 3. Throughout the simulations, all the parameters are expressed in atomic units (a.u.). In the first example of simulated potential inversion, we consider the one-dimensional O−H molecule. For purposes of illustration, the O−H bond is modeled as a Morse potential[23]

$$
V(x) = D_0[e^{-\beta(x-x_0)} - 1]^2 - D_0 \tag{31}
$$

where $D_0 = 0.1994$, $\beta = 1.189$, and $x_0 = 1.821$; virtually any model should be suitable for algorithmic testing purposes and the ones utilized here were chosen for convenience. In the simulation, the analytical bound state eigenfunctions for the Morse potential are used to construct the "experimental" probability density and energy spectral data. Then the inversion algorithm in eq 27 is applied to extract the potential.

A combination of 22 bound states with 22 arbitrary positive coefficients $c_{\{\lambda\}}$ was used in eq 27. The denominator on the RHS of eq 27 for this case is plotted in Figure 1 where none of the nodal points survives as expected. The significantly nonzero domain in Figure 1 identifies the invertible region, and the singular asymptotic regions (i.e., the regions of zero denominator) indicate where the potential may not be determined. Figure 2 compares the inverted potential from the probability density and energy spectral data by eq 27 along with the exact potential in eq 31. They are in excellent agreement in the invertible region, and no regularization was employed. As the "experimental" data in these simulations is assumed to be free of noise, for the gradient and Laplacian operations acting on the probability density, we employed the fast Fourier transform.

Under conditions of noisy data, the combined algorithm in eq 27 is also superior to that in eq 23. To illustrate the improvement of the potential inversion by eq 27 versus that
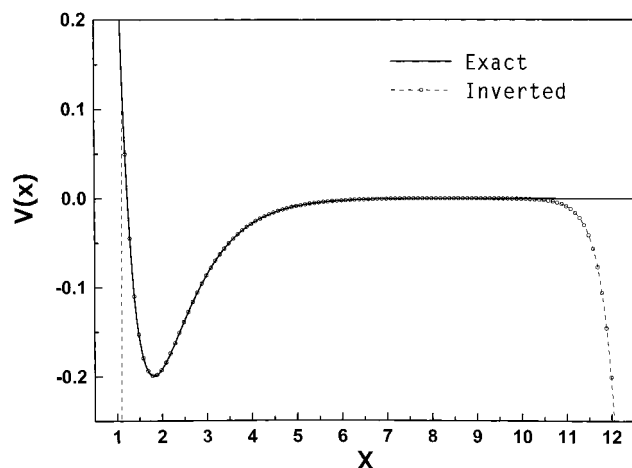
Inversion Algorithm for Quantum Systems

*J. Phys. Chem. B, Vol. 104, No. 46, 2000* **10867**



**Figure 2.** Comparison between the inverted and exact potentials in the first simulation example with perfect data by combination algorithm in eq 27. They agree very well in the invertible region.
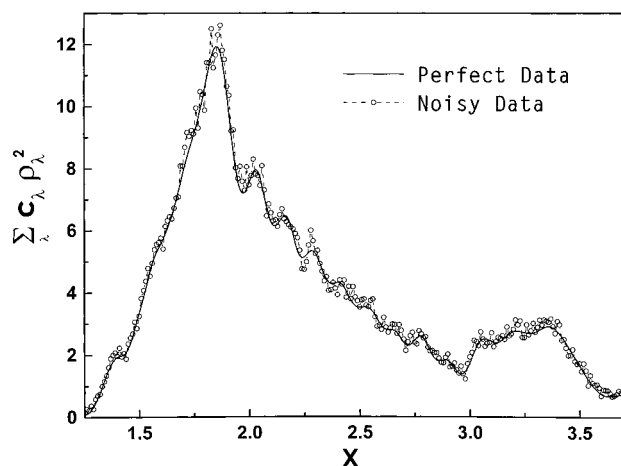


**Figure 3.** Comparison between the spatial distribution of the noisy denominator in eq 27 for the first simulation example and that of the perfect data shown in Figure 1 over the dominantly invertible domain.

for eq 23, we will consider noisy probability density data $\tilde{\rho}_n(x)$ over that of the perfect data $\rho_n(x)$ with the form:

$$\tilde{\rho}_n(x) = \tilde{\rho}_n(x) + 0.1\epsilon(x) \tag{32}$$

where $-1 \leq \epsilon(x) \leq 1$ is a rapidly fluctuating spatial function. Under the same combination of 22 bound states as above, Figure 3 compares the noisy denominator with its perfect data counterpart. Applying eq 27 will produce the noisy potential shown in Figure 4. For this noisy data inversion, the first and second derivatives in eq 27 are evaluated by a finite difference. Even with no filtering, Figure 4 shows that the potential inversion is relatively stable for noisy data in the strongly invertible regions where the spatial distribution in Figure 1 has substantial value. In the weakly invertible regions with a smaller value of the denominator in eq 27, the signal-to-noise ratio becomes smaller. Under these conditions the errors in the evaluation of the derivatives by finite differences will be larger, and thus the potential deviation will be larger. To achieve good quality inversion with noisy data, we need to combine the probability density data such that the denominator in eq 27 is large everywhere in the desired revertible region, which can optimally be done by a suitable choice of the coefficients $c_\lambda$. As a comparison with the result in Figure 4, we show in Figure 5 the inversion with noisy data of the same quality by use of the simple algorithm in eq 23 employing the second excited
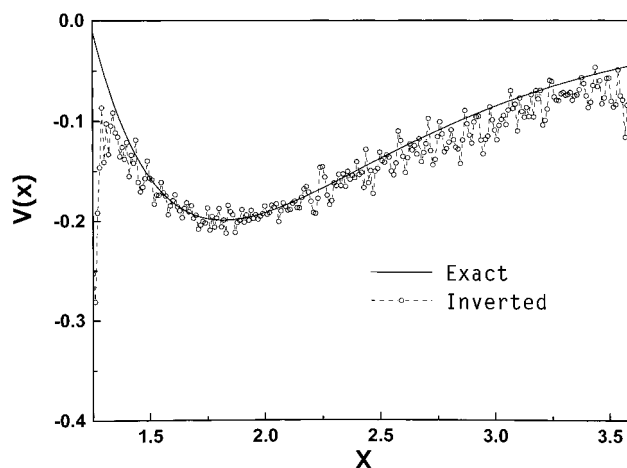


**Figure 4.** Comparison between the inverted and exact potentials in the first simulation example with noisy probability density data by the combination algorithm in eq 27. In the invertible region of large magnitude in Figure 3, the inversion is relatively stable.
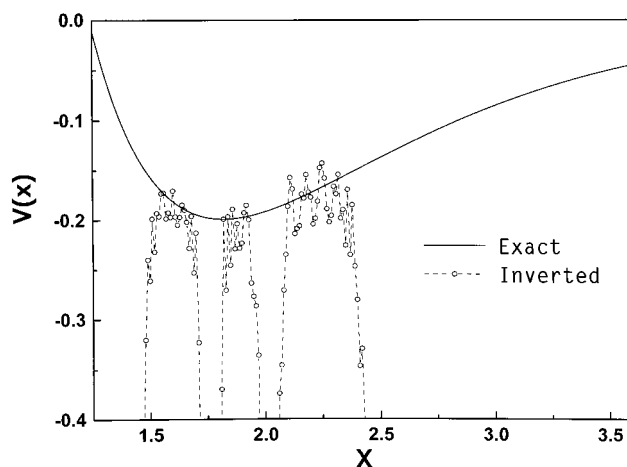


**Figure 5.** Comparison between the inverted and exact potentials in the first simulation example with noisy probability density databy the simple algorithm in eq 23. The invertible region is narrow, and the inversion in the regions around nodal points is unstable.

state $\tilde{\rho}_2(x)$. Figure 5 shows that the invertible region with eq 23 is quite narrow without taking a combination of data, and regions around nodal points are very sensitive to noise. Thus, removing the nodal points by the data combination algorithm in eq 27 greatly improves stability with noisy data. Much better results could also be obtained by more sophisticated derivative evaluation and filtering techniques. The remaining two examples will demonstrate the capabilities of eq 27 without noisy data, but the same issues are involved.

The second simulation example is a two-dimensional coupling harmonic oscillator, which is a simple model of a collinear triatomic system. The potential surface is

$$V(x_1, x_2) = \frac{1}{2}\mu_1\Omega^2 x_1^2 + \frac{1}{2}\mu^2\Omega^2 x_2^2 + \frac{1}{2}\frac{\mu_1\mu_2}{\mu_1 + \mu_2}\omega^2(x_2 - x_1)^2 \tag{33}$$

where the form of the coupling potential is chosen for convenience. The parameters are chosen corresponding to a collinear model of DOH: $\mu_1$ is the reduced mass of O−H; $x_1$ is the displacement of the O−H bond; $\mu_2$ is the atom−diatom reduced mass of the D-(OH); $x_2$ is the displacement of the D−O_H virtual bond (O_H refers the center of mass of O−H). The oscillation
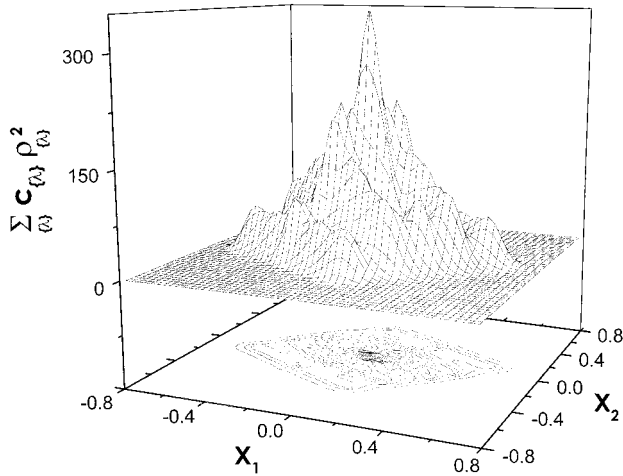
**Figure 6.** Surface and contours of the spatial distribution of the denominator in the inversion formula in the second simulation example. The significantly nonzero region defines the invertible domain.

frequencies are $\Omega = \beta\sqrt{2D_0/\mu_1}$ and $\omega = \beta\sqrt{2D_0/\mu_2}$ where $\beta$ and $D_0$ are given in the first simulation example. The Schrödinger equation is

$$\left[ -\frac{1}{2\mu_1}\frac{\partial^2}{\partial x_1^2} - \frac{1}{2\mu_2}\frac{\partial^2}{\partial x_2^2} + V(x_1, x_2) \right]\psi(x_1, x_2) = E\psi(x_1, x_2)$$
(34)

This model system has analytical eigenfunctions and eigenenergies. Specially, each eigenfunction is a product of two normalized eigenfunctions of effective one-dimensional harmonic oscillators:

$$\psi_{n',n''}(x_1, x_2) = \phi_{n'}(\alpha'x') \phi_{n''}(\alpha''x'')$$
(35)

where the quantum numbers $n'$, $n''$ are nonnegative integers. The definitions of the variables are

$$\alpha' = \sqrt{(\mu_1 + \mu_2)\Omega} \qquad \alpha'' = \sqrt{\frac{\mu_1\mu_2\sqrt{\Omega^2 + \omega^2}}{\mu_1 + \mu_2}}$$

$$x' = \frac{\mu_1 x_1 + \mu_2 x_2}{\mu_1 + \mu_2} \qquad x'' = x_2 - x_1 \quad (36)$$

The corresponding eigenenergy is

$$E_{n',n''}(\Omega, \omega) = \left(n' + \frac{1}{2}\right)\Omega + \left(n'' + \frac{1}{2}\right)\sqrt{\Omega^2 + \omega^2} \quad (37)$$

On the basis of the simulated "experimental" data of the probability density and energy spectra from eqs 35 and 37, eq 27 can be applied to invert the two-dimensional potential surface. A combination of total 25 eigenstates (i.e., $n' = 0$, 1, ..., 4; $n'' = 0$, 1, ..., 4) was chosen with arbitrary coefficients to remove the nodal lines and specify the invertible region. The dominator on the RHS of eq 27 is plotted in Figure 6 and the domain of significant magnitude identifies the invertible region. Figure 7 displays the surface and its contours for the inverted potential. For comparison, the residual between the inverted and exact potentials is plotted in Figure 8, which shows that the inversion is very accurate in the invertible region. The inversion is only ill-defined in the asymptotic regions where the probability density is uniformly very small. In this model system the eigenstates used are nondegenerate so that each eigenstate probability density is assumed to be measured separately.
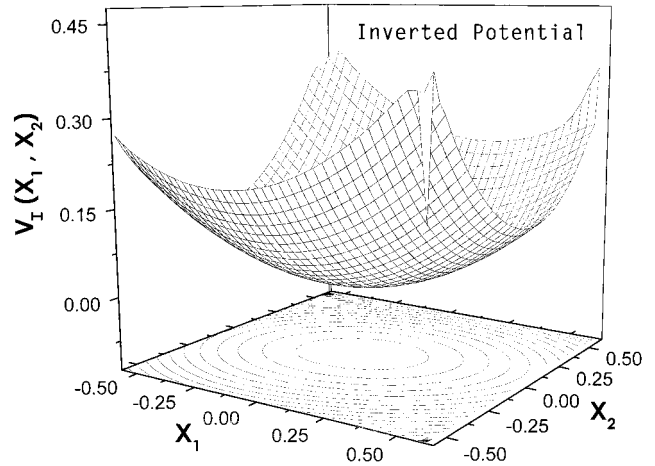


**Figure 7.** Surface and contours of the inverted two-dimensional potential in the second simulation example.
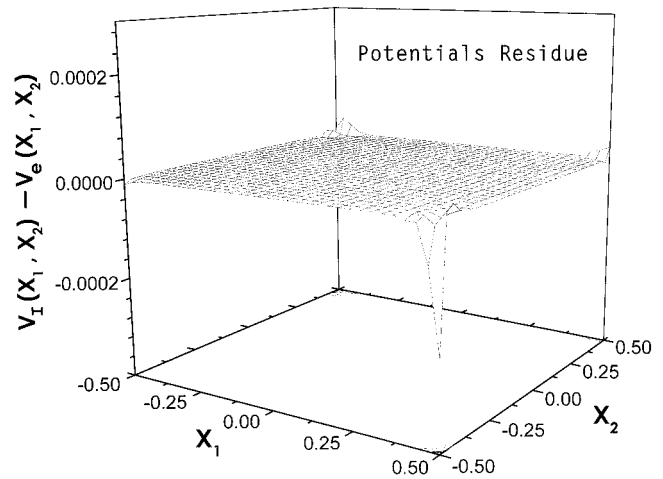


**Figure 8.** Surface and contours of the residual between the inverted and the exact potentials in the second simulation example. The result in the invertible region are very accurate.

In the third simulation, we consider a system with degenerate eigenstates. The model system is the same as that used in the second example except for a different mass $\mu_2$, which means the triatomic system DOH is replaced by $\Lambda$OH. Supposing the abstract atom $\Lambda$ is lighter than H to result in $\mu_2 = 4\mu_1/5$, then we will have the energy spectra as

$$E_{n',n''}(\Omega) = \left(n' + \frac{1}{2}\right)\Omega + \frac{3}{2}\left(n'' + \frac{1}{2}\right)\Omega \qquad (38)$$

Choosing the same combination of 25 eigenstates for inversion as used in the second example, we find that there are 6 pairs of degenerate eigenstates: $(\psi_{0,2}, \psi_{3,0})$, $(\psi_{0,3}, \psi_{3,1})$, $(\psi_{0,4}, \psi_{3,2})$, $(\psi_{1,2}, \psi_{4,0})$, $(\psi_{1,3}, \psi_{4,1})$, $(\psi_{1,4}, \psi_{4,2})$. In the simulation, we assume that the two components in the pair of degenerate eigenstates cannot be distinguished during excitation, but a specified excitation will result in a particular and reproducible superposition of the two components in the degenerate state. In the simulation, we assigned arbitrary superpositions for each of the 6 pairs of degenerate eigenstates as

$$\psi(x_1, x_2) =$$

$$\frac{c_1}{\sqrt{c_1^2 + c_2^2}}\psi_{n_1',n_3''}(x_1, x_2) + \frac{c_2}{\sqrt{c_1^2 + c_2^2}}\psi_{n_2',n_4''}(x_1, x_2) \quad (39)$$

Inversion Algorithm for Quantum Systems

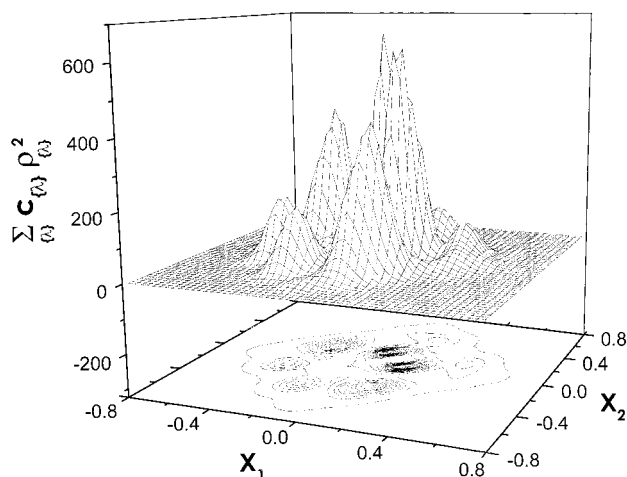*J. Phys. Chem. B, Vol. 104, No. 46, 2000* **10869**



**Figure 9.** Surface and contours of the spatial distribution of the denominator in the inversion formula in the third simulation example. The significantly nonzero region defines the invertible domain.
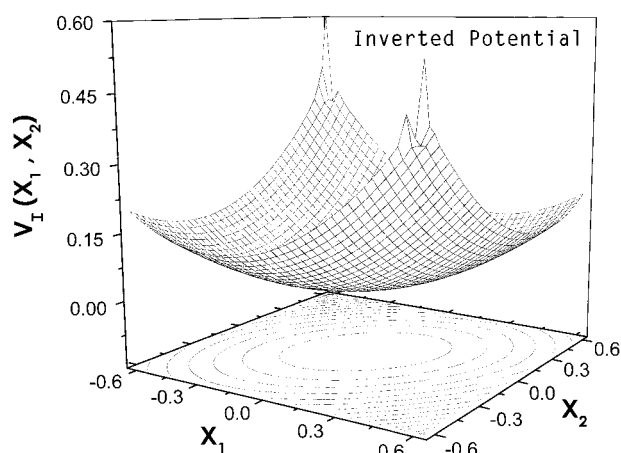


**Figure 10.** Surface and contours of the inverted two-dimensional potential in the third simulation example.
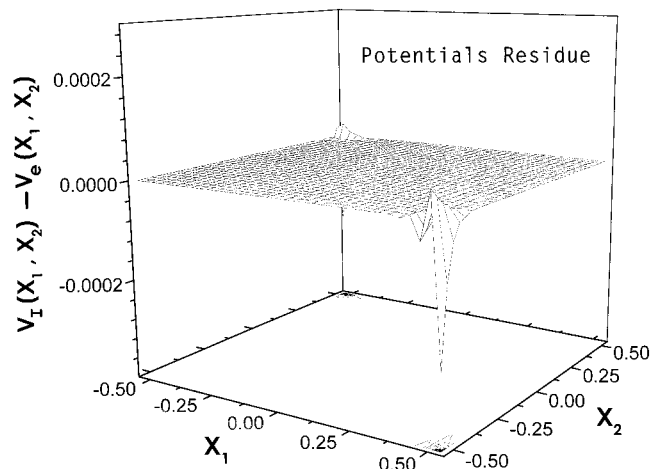


**Figure 11.** Surface and contours of the residual between the inverted and the exact potential in the third simulation example.

where $\psi_{n_1',n_3''}(x_1, x_2)$ and $\psi_{n_2',n_4''}(x_1, x_2)$ are degenerate and $c_1$ and $c_2$ are real coefficients. Using this combination, the denominator on the RHS of eq 27 is plotted in Figure 9, where the probability density of the superposition is very different from that of a pure eigenstate combination in Figure 6. Figure 10 is the surface and contours of the inverted potential. Once again, the invertible region can be estimated from the significantly nonzero domain in Figure 9. Figure 11 shows the residual error between the

inverted and exact potentials. As expected, even when a degenerate superposition of probability densities is used in eq 27, the inverted potential agrees with the exact potential very well in the stable region.

## 5. Summary

This paper first derived a time dependent algorithm for multidimensional potential inversion with probability density data in terms of a linear integral equation formulation. The one-dimensional version of this algorithm has been successfully tested elsewhere. Ultrafast multidimensional probability density data are presently not available, and the latter algorithm can involve considerable computational effort. Thus, a new time independent multidimensional inversion algorithm was investigated for its viability.

The analysis revealed that the time independent multidimensional algorithm in eq 13, as an analogue of its time dependent counterpart, will fail if only real bound eigenstates are involved. The reason for this behavior is that when the time dependent probability density goes over to its time independent counterpart, the relative phases among different eigenstates are lost, and a global inversion singularity emerges. The global singularity prevents identification of the true potential by inversion of probability density data in terms of a linear integral equation formulation.

To deal with the global singularity problem, a direct time independent multidimensional algorithm was developed to achieve the potential inversion. However, the simple formulation in eq 23 encounters unstable behavior in the nodal regions. A modified version in eq 27 circumvents the instability in the nodal regions, to permit the extraction of the full multidimensional potential in any invertible region. This time independent inversion algorithm relies on emerging high resolution eigenstate probability density and energy spectral data. The algorithm was successfully tested for the inversion of one- and two-dimensional model systems. The singular behavior at the nodal points usually can be eliminated by combining data from a few eigenstate probability densities which do not share common nodal surfaces. The only requirement for the system is that the eigenfunction be real, which usually is satisfied under sufficient physical boundary conditions. We hope that this work serves to further stimulate experimental efforts aimed at generating probability density data.

Finally, it is instructive to consider the direct algorithm presented in eqs 23, 26, or 27 and its relation to the loss of phase in the probability density. Although $\psi(\mathbf{x})$ is not a proper physical observable, if it was know then simple devision of the Schrödinger equation (9) by $\psi(\mathbf{x})$ would give a direct expression for the potential: $V(\mathbf{x}) = E + [2\psi(\mathbf{x})]^{-1}\nabla^2\psi(\mathbf{x})$. Measurement of $\rho(\mathbf{x}) = |\psi(\mathbf{x})|^2$ destroys the wave function phase and prevents direct use of the latter formulation on nodal regions. The results in eqs 23, 26, or 27 circumvent the singular trouble on nodal regions to fully prescribe the potential.

## References and Notes

(1) Ischtwan, J.; Collins, M. *J. Chem. Phys.* **1994**, *100*, 8080.

(2) Ho, T.; Rabitz, H. *J. Chem. Phys.* **1996**, *104*, 2584.

(3) Lowe, B.; Pilant, M.; Rundell, W. *SIAM (Soc. Ind. Appl. Math.) J. Math. Anal.* **1992**, *23*, 482.

(4) Fabiano, R.; Knobel, R.; Lowe, B. *IMA J. Numer. Anal.* **1995**, *15*, 75.

(5) *Quantum Inversion Theory and Applications*; von Geramb, H. V., Eds.; Springer: New York, 1994.

(6) Ho, T.; Rabitz, H. *J. Phys. Chem.* **1993**, *97*, 13447.

(7) Ho, T.; Rabitz, H.; Choi, S.; Lester, M. *J. Chem. Phys.* **1996**, *104*, 1187.

(8) Zhang, D.; Light, J. *J. Chem. Phys.* **1995**, *103*, 9713.

(9) Zewail, A. *J. Phys. Chem.* **1993**, *97*, 12427.

(10) Stapelfeldt, H.; Constant, E.; Sakai, H.; Corkum, P. *Phys. Rev. A* **1998**, *58*, 426.

(11) Geiser, J.; Weber, P. *J. Chem. Phys.* **1998**, *108*, 8004.

(12) Williamson, J.; Cao, J.; Ihee, H.; Frey, H.; Zewail, A. *Nature (London)* **1997**, *386*, 159.

(13) Krause, J.; Schafer, K.; Ben-Nun, M.; Wilson, K. *Phys. Rev. Lett.* **1997**, *79*, 4978.

(14) Jones, R. *Phys. Rev. A* **1998**, *57*, 446.

(15) Assion, A.; Geisler, M.; Helbing, J.; Seyfried, V.; Baumert, T. *Phys. Rev. A* **1996**, *54*, R4604.

(16) Vager, Z.; Naaman, R.; Kanter, E. *Science* **1989**, *244*, 426.

(17) Kwon, K.; Moscowitz, A. *Phys. Rev. Lett.* **1996**, *77*, 1238.

(18) Zhu, W.; Rabitz, H. *J. Chem. Phys.* **1999**, *111*, 472.

(19) Baer, R.; Kosloff, R. *J. Phys. Chem.* **1995**, *99*, 2534.

(20) Lu, Z.; Rabitz, H. *Phys. Rev. A* **1995**, *52*, 1961.

(21) Shapiro, M. *J. Phys. Chem.* **1996**, *100*, 7859.

(22) Bohm, D. *Phys. Rev.* **1952**, *85*, 166.

(23) Paramonov, G. K. *Chem. Phys.* **1993**, *177*, 169.